Magnetism, transport, and specific heat of electronically phase-separated $Pr_{0.7}Pb_{0.3}MnO_3$ single crystals

2009 J. Phys.: Condens. Matter 21 076002

(http://iopscience.iop.org/0953-8984/21/7/076002)

J. Phys.: Condens. Matter **21** (2009) 076002 (6pp) doi:10.1088/0953-8984/21/7/076002

Magnetism, transport, and specific heat of electronically phase-separated $Pr_{0.7}Pb_{0.3}MnO_3$ single crystals

Run-Wei Li[1,4], **Alexei A Belik**[2], **Zhi-Hong Wang**[3] and **Bao-Gen Shen**[3]

[1] Ningbo Institute of Materials Technology and Engineering (NIMTE), Chinese Academy of Sciences (CAS), Ningbo, Zhejiang 315201, People's Republic of China
[2] International Center for Materials Nanoarchitectonics (MANA), National Institute for Materials Science (NIMS), 1-1 Namiki, Tsukuba, Ibaraki 305-0044, Japan
[3] State Key Laboratory of Magnetism, Institute of Physics and Center for Condensed Matter Physics, Chinese Academy of Sciences (CAS), PO Box 603, Beijing 100080, People's Republic of China

Received 15 September 2008, in final form 28 December 2008
Published 23 January 2009
Online at stacks.iop.org/JPhysCM/21/076002

Abstract

Magnetization, resistivity, and specific heat were studied systematically in the absence and presence of magnetic field in $Pr_{0.7}Pb_{0.3}MnO_3$ single crystals, in which electronic phase separation occurs near the ferromagnetic/metallic-paramagnetic/insulating phase transition and the metal–insulator transition temperature is much higher than the Curie temperature. These measurements allow us to extract some fundamental physical parameters such as Fermi energy, density of states at the Fermi energy, Debye temperature, and interaction among electrons, phonons, and magnons. Furthermore, the magnetic entropy was studied around the phase transition temperature regime. It was found that a magnetic entropy change associated with the transition from the connected ferromagnetic phase to isolated superparamagnetic clusters appeared near the metal–insulator transition temperature following a large magnetic entropy change near the ferromagnetic–paramagnetic phase transition.

(Some figures in this article are in colour only in the electronic version)

1. Introduction

Since the discovery of colossal magnetoresistive effects (CMR) [1, 2], a significant decrease of resistivity induced by applying magnetic field, perovskite manganites $Ln_{1-x}A_xMnO_3$ (Ln = La, Pr, Nd . . . , A = Ca, Sr, Ba, Pb . . .) have been studied extensively due to not only their rich physical properties but also potential applications in magnetic sensors. It is believed that the coexistence and competition between different interactions among charge, lattice, orbital, and spin degrees of freedom result in many observed fascinating phenomena. In addition, microscopic electron phase separation has also been found in manganites [3–8], which gives rise to further complication in understanding the underlying physics. For example, in the typical double exchange system $La_{0.67}Ca_{0.33}MnO_3$, when the temperature is slightly above the Curie temperature, ferromagnetic clusters separate from the paramagnetic insulating matrix [9, 10]. These ferromagnetic clusters are several nanometers in size and probably a regular distribution due to the extended Coulomb interaction within and among ferromagnetic clusters. The competition between double exchange, super-exchange, Coulomb coupling, interfacial energy, etc determines the specific size, shape, and distribution of the coexisting phases in electronically phase-separated systems.

In our previous studies [11, 12], it was found that single crystalline $Pr_{0.7}Pb_{0.3}MnO_3$ indicated an electronic phase separation near the metal–insulator transition temperature (T_p, ∼235 K). With increasing temperature, this system experienced an unconventional sequence of phase transition processes, ferromagnetic phase → ferromagnetic + paramagnetic phase → superparamagnetic + paramagnetic phase → paramagnetic phase. Moreover, in the temperature region

[4] Author to whom any correspondence should be addressed.

slightly above T_p, a large low-field magnetoresistance due to the spin-dependent electron tunneling between ferromagnetic clusters was observed [11]. The phase transition process is different from conventional second order phase transition due to the process dependence of transport properties [12]. Furthermore, such an unconventional phase transition process has been verified directly by means of variable-temperature scanning tunneling microscopy [13].

To better understand the electronic properties of the electronically phase-separated systems and the underlying mechanism, it is crucial to carefully investigate the phase transition process and the fundamental physical properties especially at low temperature. In this paper, specific heat, magnetization, and resistivity were measured systematically in $Pr_{0.7}Pb_{0.3}MnO_3$ single crystals in the absence and presence of magnetic fields. Based on these measurements, some fundamental physical parameters such as Fermi energy, density of states at the Fermi energy $N(E_F)$, Debye temperature θ_D, and major interaction among electrons, phonons, and magnons at low temperature have been extracted. Furthermore, the magnetic entropy was studied in the phase separation temperature range by both the magnetization and specific heat measurements.

2. Experimental details

$Pr_{0.7}Pb_{0.3}MnO_3$ single crystals grown by the flux method have been used in our previous studies [11, 12]. Specific heat, C_p versus T, was recorded between 1.8 and 300 K in the presence and absence of the magnetic field by a pulse relaxation method using a commercial calorimeter (Quantum Design PPMS, physical property measurement system). The sample was attached to a sapphire plate using an Apiezon grease. The magnetic properties were measured by a superconductive quantum interference device (SQUID, Quantum Design). Electrical transport properties were measured by a standard four-probe method by the *PPMS*.

3. Results and discussion

3.1. Phase transition and magnetic entropy change

Figure 1(a) shows the temperature dependence of magnetization and resistance. The sample shows a transition from a ferromagnetic to paramagnetic phase at 205 and 278 K under a field of 0.1 and 5 T, and a metal–insulator transition at 235 and 280 K under a field of 0 and 5 T, respectively. It is noteworthy that T_p, which is defined as the temperature corresponding to the resistance peak in the R–T curve, is higher than the Curie temperature (T_C) under a low magnetic field. The complicated phase transition process has been investigated by magnetization, transport, and electron spin resonance measurements in our previous studies [11, 12]. The specific heat as a function of temperature measured under a magnetic field of 0 and 5 T is shown in figure 1(b). At low temperature, the specific heat value is almost independent of the magnetic field. At room temperature, the specific heat is around 115 J mol^{-1} K^{-1}, in good agreement with other specific

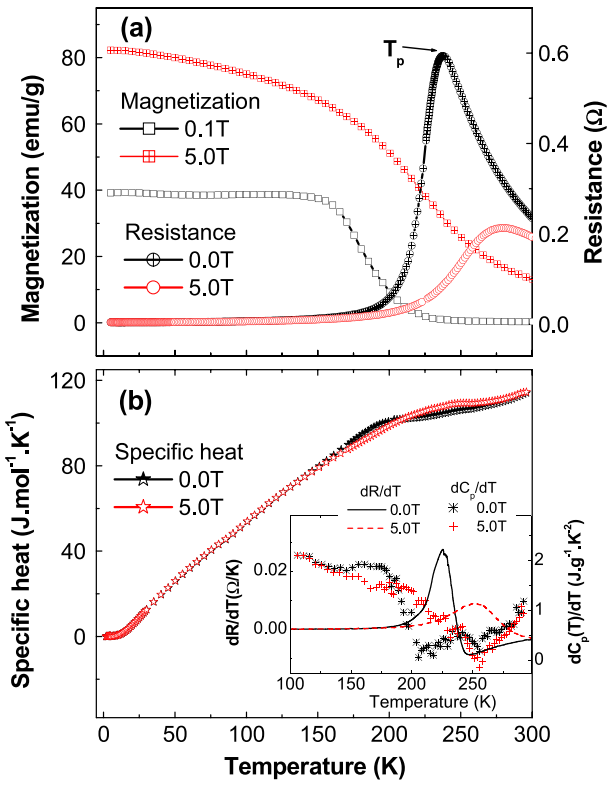

Figure 1. Temperature dependence of (a) magnetization and resistivity, and (b) specific heat. The inset of (b) shows the differential of resistivity (dR/dT) and specific heat (dC_p/dT) as a function of temperature under a magnetic field of 0 and 5 T, respectively.

heat measurements in this type of materials. There are no clear peaks or discontinuity in the specific heat versus temperature curves around T_C, which indicates that the phase transition is second order. As shown in the inset of figure 1(b), when we compare the differential of resistivity (dR/dT), and specific heat (dC_p/dT), at the temperature where a peak appears in the dR/dT–T curves (the sharpest temperature point in the R–T curves), a broad peak in dC_p/dT–T was observed as well. The peaks in the dC_p/dT–T curves move towards high temperature with the applied field. In other words, while the metal–insulator transition occurs, the specific heat changes correspondingly though very little.

Isothermal magnetization curves were recorded in the temperature regime from 180 to 280 K, which covers the ferromagnetic–paramagnetic and metal–insulator phase transitions. The temperature interval of 2.5 K was employed in the aforementioned measurements. Figure 2 shows Arrott plots with a temperature interval of 5 K (in order to be clear). Magnetic behaviors can be well studied by analyzing Arrott plots [14, 15] at temperature around T_C. In Arrott plots, the M^2 versus $\mu_0 H/M$ curves should be straight lines in the high magnetic field range. The intercept of the M^2 versus $\mu_0 H/M$ curves on the $\mu_0 H/M$ axis is negative/positive below/above T_C. In other words, at T_C, the extrapolation of the M^2 versus $\mu_0 H/M$ curve should pass through zero on the $\mu_0 H/M$ axis. Based on this method, the T_C of the $Pr_{0.7}Pb_{0.3}MnO_3$ single crystal was determined to be around 205 K, and the phase

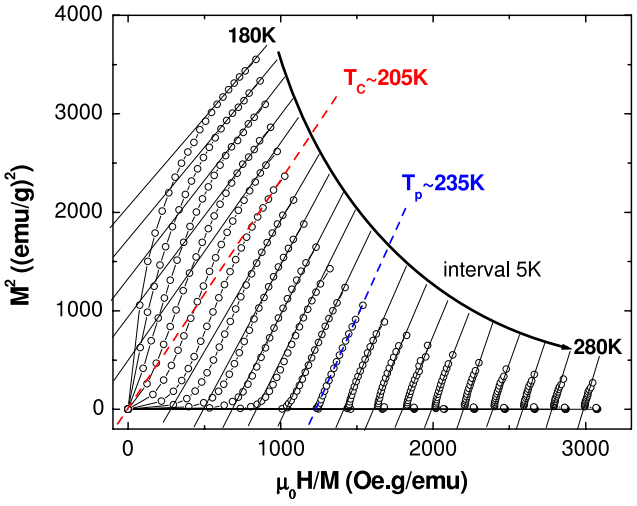

Figure 2. Arrott plots measured from 180 to 280 K.

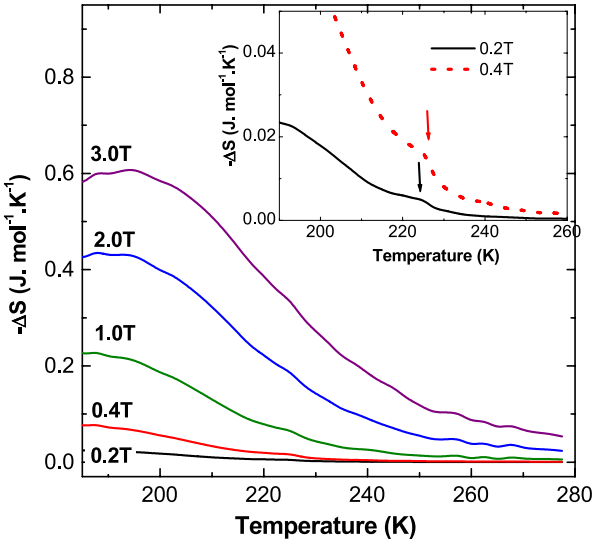

Figure 3. Temperature dependence of the magnetic entropy change under a magnetic field change of 0.2, 0.4, 1.0, 2.0, and 3.0 T, respectively. The inset is the magnification of that with the magnetic field of 0.2 and 0.4 T.

transition is second order because the slopes of all the M^2 versus $\mu_0 H/M$ curves are positive. Additionally, M^2 versus $\mu_0 H/M$ curves change their shapes from a reversed 'L' below 235 K into an 'L' shape above 235 K. At 235 K, the metal–insulator transition temperature (see figure 1(a)), the M^2 versus $\mu_0 H/M$ curve becomes a simple straight line from low to high magnetic field. Similar behaviors were also observed in $La_{0.67}Ca_{0.33}MnO_3$ polycrystalline samples with a T_C of 265 K, though no details have been discussed on the anomalous behaviors yet [16]. It seems that the metal–insulator transition may be reflected from the Arrott plots. We are investigating this issue in other systems and will report in more detail elsewhere.

The magnetic entropy change during the second order phase transition can be calculated by

$$\Delta S_{\mathrm{M}}(T, \Delta H) = \int_{H_I}^{H_{\mathrm{F}}} \mathrm{d}S_{\mathrm{M}}(T, H)_T$$

$$= \int_{H_I}^{H_{\mathrm{F}}} \left[\frac{\partial M(T, H)}{\partial T}\right]_H \mathrm{d}H. \qquad (1)$$

Figure 3 shows the magnetic entropy change as a function of temperature derived from equation (1). The maximum of the magnetic entropy change appears around T_C; $|-\Delta S_M|$ is 0.6 J mol^{-1} K^{-1} at 200 K with a magnetic field change of 3 T. The low value of the magnetic entropy change can be attributed to the short range correlations in the superparamagnetic clusters, as suggested by electron spin resonance data as well as a deviation of the inverse magnetization versus temperature from the Curie–Weiss law reported in our previous papers [11, 12]. This is in good agreement with other systems, such as $La_{1-x}Ca_xMnO_3$ and so on [17–19]. Kinks appear in the $-\Delta S_M$ versus T curves around 224 K, which is much clearer under low magnetic fields, i.e. 0.2 or 0.4 T, as magnified in the inset of figure 3. What should be noted is that the $\mathrm{d}Cp/\mathrm{d}T$–T and $\mathrm{d}R/\mathrm{d}T$ curves with a zero magnetic field also indicate peaks around 224 K (see figure 1(b)). At this temperature, according to our previous studies by magnetization, resistivity, and electron spin resonance measurements [11, 12], the connected ferromagnetic metallic phases transform into isolated

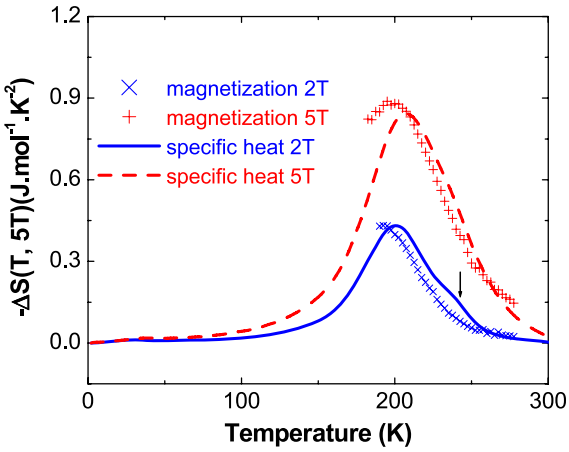

Figure 4. Temperature dependences of magnetic entropy changes calculated from magnetization and specific heat measurements.

ferromagnetic clusters, which behave as superparamagnetic clusters due to the thermal fluctuation. Therefore, the entropy changes between the connected ferromagnetic phases and the isolated superparamagnetic clusters must be responsible for the kinks observed in the inset of figure 3.

The magnetic entropy change can also be calculated based on specific heat measurements with and without magnetic fields according to

$$\Delta S_{\mathrm{heat}}(T, \Delta H) = \int_0^T [C_p(T, H) - C_p(T, 0)]\frac{\mathrm{d}T}{T} \qquad (2)$$

where $C_p(T, H)$ and $C_p(T, 0)$ are the specific heat at temperature T and under a magnetic field of H and 0 T, respectively. The entropy changes as a function of temperature with a magnetic field change of 2 and 5 T, respectively, were calculated and shown in figure 4. The magnetic entropy

Table 1. Fit parameters of low-temperature specific heat.

	γ (mJ K^{-2} mol^{-1})	β_3 (mJ K^{-4} mol^{-1})	β_5 (mJ K^{-6} mol^{-1})	Θ_D (K)
0 T	8.2	0.26	2.28×10^{-3}	334.5
2 T	7.4	0.28	2.17×10^{-3}	326.3
5 T	7.2	0.29	2.12×10^{-3}	322.4

changes calculated from the magnetization and specific heat are well consistent with each others in values, though the temperatures where the maximum of ΔS appears shift slightly from each other, possibly due to the different measuring systems. With the magnetic field change of 2 T, there is a clear upheaval in the magnetic entropy change calculated from the specific heat data around 240 K, which is around the T_p under a magnetic field of 2 T. This agrees well with the fact that there is a magnetic entropy change, even though not big, around the metal–insulator transition (as shown in the inset of figure 3) associated with the transition from the connected ferromagnetic metallic phase to isolated superparamagnetic clusters. Under a high magnetic field, i.e. 5 T, the upheaval of ΔS at the T_{MI} is concealed in the peak at the T_C.

3.2. Low-temperature magnetization, resistivity, and specific heat

Figure 5 shows the temperature dependence of the low-temperature specific heat of $Pr_{0.7}Pb_{0.3}MnO_3$ single crystals. We have fitted these data by

$$C_p = C_{lat} + C_{ele} + C_{mag}. \quad (3)$$

The phonon contribution arising from lattice vibration can be described as $C_{lat} = \beta_3 T^3 + \beta_5 T^5$. The electric contribution due to the free charges can be written as $C_{ele} = \gamma T$. The magnetic term due to the spin wave contribution can be written as $C_{mag} = \delta T^{\frac{3}{2}}$. The hyperfine term caused by the level splitting induced by local magnetic field at the Mn and Pr nuclear spins, which usually appears at very low temperature, was neglected. Thus the low-temperature specific heat data were modeled by

$$C(T) = \gamma T + \delta T^{\frac{3}{2}} + \beta_3 T^3 + \beta_5 T^5. \quad (4)$$

Under a magnetic field of 0, 2, and 5 T, respectively, the fitting parameters are shown in table 1. γ of $Pr_{0.7}Pb_{0.3}MnO_3$ single crystals is larger than that of $La_{0.7}Sr_{0.3}MnO_3$ (3.39 mJ K^{-2} mol^{-1}) [20] and $La_{0.7}Ba_{0.3}MnO_3$ (6.1 mJ K^{-2} mol^{-1}) [21] and smaller than that of $Pr_{0.63}Ca_{0.37}MnO_3$ (11 mJ K^{-2} mol^{-1}) [22] and $Pr_{0.7}Ca_{0.3}MnO_3$ (30.6 mJ K^{-2} mol^{-1}) [23], but similar to $Y_{0.7}Sr_{0.3}MnO_3$ (8.1 mJ K^{-2} mol^{-1}) [7]. If we assume that the linear term in the specific heat arises from the charge carrier completely, we can compute the density of states $N(E)$ at the Fermi energy E_F according to $\gamma = \frac{\pi^2}{3} k_B^2 N(E_F)$, $N(E_F) = 6.0 \times 10^{22}$ eV cm^{-3} with $\gamma = 8.2$ mJ K^{-2} mol^{-1}. For a free electron gas, $N(E_F) = \frac{3n}{2E_F}$; n is the carrier concentration and should be 1.2×10^{22} cm^{-3} in $Pr_{0.7}Pb_{0.3}MnO_3$ single crystals assuming all holes induced by the dopants are mobile carriers. Thus we have $E_F = 0.30$ eV.

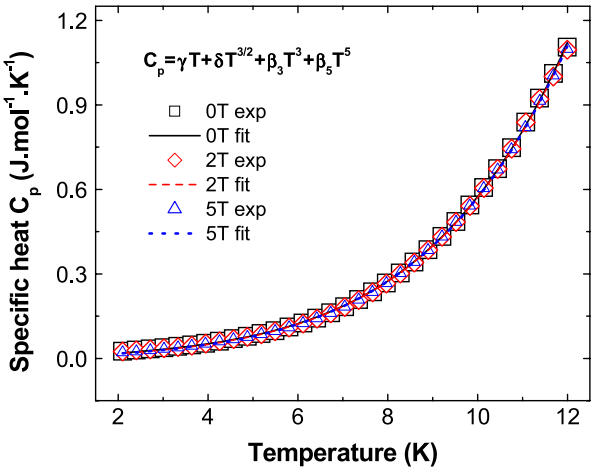

Figure 5. Low-temperature specific heats measured under a magnetic field of 0, 2, and 5 T, respectively. The scatter plot is experimental data points, and the lines are the fitting results based on $C(T) = \gamma T + \delta T^{\frac{3}{2}} + \beta_3 T^3 + \beta_5 T^5$.

According to the lattice term, the obtained β_3 is 0.26 mJ K^{-4} mol^{-1}, basically consistent with a normal value associated with the lattice contribution (0.1–0.2 mJ K^{-4} mol^{-1}) [5, 24–26]. From β we can obtain *Debye* temperature Θ_D = 334.5, 326.3, and 322.4 K under a magnetic field of 0, 2, and 5 T, respectively, based on the standard expression $\Theta_D = (12\pi^4 PR/5\beta_3)^{\frac{1}{3}}$, where $P = 5$ is the number of atoms in each molecule, and R is the ideal gas constant.

In our fit above, no magnetic contribution to the low-temperature specific heat was found, which is consistent with the results reported by Hamilton *et al* [23]. The spin wave excitation was investigated by fitting the low-temperature magnetization data. Figure 6 shows the low-temperature magnetization as a function of temperature measured under a magnetic field of 5 T. The experimental data were fitted by $\frac{M(T)}{M(5\text{ K})} = 1 - BT^n$, where B and n are fitting parameters. When we fitted the data in the temperature range from 5 to 90 K, $B = 3.0 \times 10^{-5}$ K$^{-3/2}$ with $n = 1.71$, basically consistent with the fitting parameters from 5 to 150 K ($B = 3.0 \times 10^{-5}$ K$^{-3/2}$ with $n = 1.74$). When we narrow the fitting temperature range, B becomes smaller while n becomes bigger; i.e., between 5 and 60 K $B = 2.0 \times 10^{-5}$ K$^{-3/2}$ with $n = 1.87$, and between 5 and 40 K $B = 6.5 \times 10^{-6}$ K$^{-3/2}$ with $n = 2.16$. This is quite different from the Bloch $T^{3/2}$ law due to spin wave excitation. The fitting results indicate that the spin wave excitation at low temperature is negligible, which is well consistent with the low-temperature specific heat results.

Figure 7 shows the temperature dependence of the low-temperature resistivity under a magnetic field of 0, 2.4, and 5 T, respectively. In the temperature range below $0.5T_C$

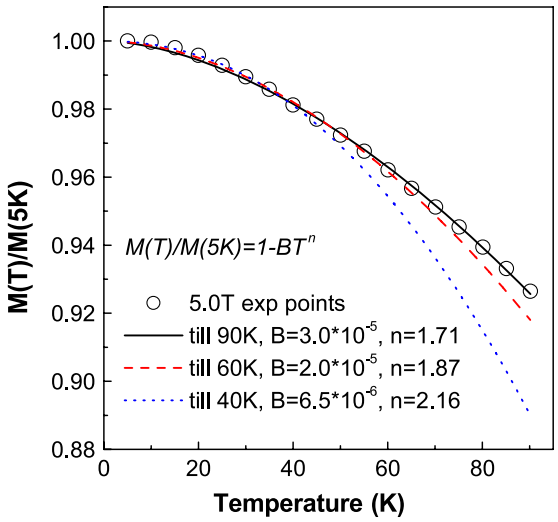

Figure 6. Normalized low-temperature magnetization under a magnetic field of 5 T. The scatter plot is experimental data points. The experimental data were fitted by $\frac{M(T)}{M(5\ \mathrm{K})} = 1 - BT^n$ from 5 to 90 K (solid line), to 60 K (dashed line), and to 40 K (dotted line), respectively.

Table 2. Fit parameters of low-temperature resistivity. $\rho = \rho_0 + AT^\alpha$.

	ρ_0 (Ω cm)	A (Ω cm K$^{-\alpha}$)	α
0 T	3.90×10^{-4}	1×10^{-8}	2.13 ± 0.06
2.4 T	3.90×10^{-4}	2×10^{-8}	2.02 ± 0.05
5 T	3.93×10^{-4}	2×10^{-8}	2.02 ± 0.06

($T_C \sim 205$ K), the resistivity was well fitted by $\rho = \rho_0 + AT^\alpha$ with ρ_0, A, and α free parameters, where ρ_0 is the residual resistivity that is considered as a measurement of the effective disorder, and AT^α a generic *T-power* law, which can be used to simulate different scattering processes. The fitting results are shown by solid lines in figure 7. The fit parameters are listed in table 2. The residual resistivity ρ_0 is 3.9×10^{-4} Ω cm, and basically independent of the magnetic field, which suggests that magnetic defects/impurities as well as magnetic domain walls do not contribute significantly to the residual resistivity in the manganite single crystals. As is well known, the $T^{2.5}$ term in the low-temperature resistivity is an empirical fit to the data which represents a combination of electron–electron, electron–phonon, and electron–magnon scattering, and the T^2 term is mainly due to the electron–electron scattering [27]. Our fitting results show that α is 2.13 without magnetic field and decreases to 2.02 under a magnetic field of 2 and 5 T. This suggests that the electron–electron coupling is very strong. Moreover, we have tried to fit the low-temperature resistivity by $\rho = \rho_0 + aT^2 + bT^{3.5} + aT^{4.5} + aT^5$, where $T^{3.5}$ is due to spin wave scattering [28], $T^{4.5}$ is due to electron–magnon scattering [29], and T^5 is due to electron–phonon scattering [30]. The fitting results are not better than that based on $\rho = \rho_0 + AT^\alpha$. Moreover, the main contribution is from the T^2 term. As a result, the electron–electron interactions are dominant at low temperature.

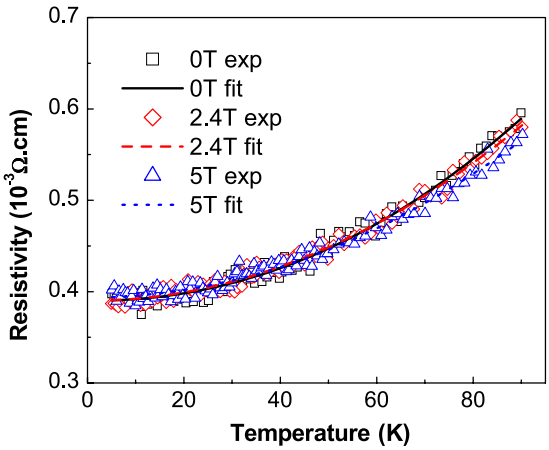

Figure 7. Low-temperature resistivity measured under a magnetic field of 0, 2.4, and 5 T, respectively. The scatter plot is experimental data points, and the lines are the fitting results based on $\rho = \rho_0 + AT^\alpha$.

4. Summary

In $Pr_{0.7}Pb_{0.3}MnO_3$ single crystals, in which electronic phase separation occurs near the ferromagnetic/metallic-paramagnetic/insulating phase transition, the magnetic entropy was studied around the phase transition temperature regime. It was found that a magnetic entropy change associated with the transition from the connected ferromagnetic phase to isolated superparamagnetic clusters appeared near the metal–insulator transition temperature following a large magnetic entropy change near the ferromagnetic–paramagnetic phase transition. Moreover, by means of measuring the low-temperature magnetization, resistivity, and specific heat, fundamental physical parameters such as the Fermi energy, the density of states at the Fermi energy, and the Debye temperature θ_D have been extracted experimentally. By fitting the low-temperature magnetization, resistivity, and specific heat as functions of temperature, electron–electron interaction was found to be dominant at low temperature.

Acknowledgments

The authors acknowledge financial support from the Ministry of Science and Technology of China, the National Natural Science Foundation of China, and MEXT in Japan (World Premier International Research Center Initiative on Materials Nanoarchitectonics).

References

[1] von Helmolt R, Wecker J, Holzapfel B, Schultz L and Samwer K 1993 *Phys. Rev. Lett.* **71** 2331
[2] Jin S, Tiefel T H, McCormack M, Fastnacht R A, Ramesh R and Chen L H 1994 *Science* **264** 413
[3] Moreo A, Yunoki S and Dagotto E 1999 *Science* **283** 2034
[4] Papavassiliou G, Fardis M, Belesi M, Maris T G, Kallias G, Pissas M, Niarchos D, Dimitropoulos C and Dolinsek J 2000 *Phys. Rev. Lett.* **84** 761

[5] Allodi G, De Renzi R, Licci F and Pieper M W 1998 *Phys. Rev. Lett.* **81** 4736
[6] Uehara M, Mori S, Chen C H and Cheong S-W 1999 *Nature* **399** 560
[7] Fäth M, Freisem S, Menovsky A A, Tomioka Y, Aarts J and Mydosh J A 1999 *Science* **285** 1540
[8] Mori S, Chen C H and Cheong S-W 1998 *Phys. Rev. Lett.* **81** 3972
[9] De Teresa J M, Ibarra M R, Algarabel P A, Ritter C, Marquina C, Blasco J, Garsia J, del Moral A and Arnold Z 1997 *Nature* **386** 256
[10] Goodenough J B and Zhou J-S 1997 *Nature* **386** 229
[11] Li R-W, Wang Z-H, Wang W-N, Sun J-R, Li Q-A, Zhang S-Y, Cheng Z-H and Shen B-G 2002 *Appl. Phys. Lett.* **80** 3367
[12] Li R-W, Zhou X, Shen B-G and Hillebrands B 2005 *Phys. Rev.* B **71** 092407
[13] Roessler S, Ernst S, Padmanabhan B, Elizabeth S, Bhat H L, Wirth S and Steglich F 2007 *IEEE Trans. Magn.* **43** 3064
[14] Arrott A 1957 *Phys. Rev.* **108** 1394
[15] Yeung I, Roshko R M and Williams G 1986 *Phys. Rev.* B **34** 3456
[16] Moutis N, Panagiotopoulos I, Pissas M and Niarchos D 1999 *Phys. Rev.* B **59** 1129
[17] Jia L, Liu G J, Wang J Z, Sun J R, Zhang H W and Shen B G 2006 *Appl. Phys. Lett.* **89** 122515
[18] Kim D, Revaz B, Zink B L, Hellman F, Rhyne J J and Mitchell J F 2002 *Phys. Rev. Lett.* **89** 227202
[19] Egilmez M, Chow K H, Jung J, Fan I, Mansour A I and Salman Z 2008 *Appl. Phys. Lett.* **92** 132505
[20] Woodfield B F, Wilson M L and Byers J M 1997 *Phys. Rev. Lett.* **78** 3201
[21] Coey J M D, Viret M, Ranno L and Ounadjela K 1995 *Phys. Rev. Lett.* **75** 3910
[22] Hardy V, Wahl A, Martin C and Simon Ch 2001 *Phys. Rev.* B **63** 224403
[23] Smolyaninova V N, Biswas A, Zhang X, Kim K H, Kim B-G, Cheong S-W and Greene R L 2000 *Phys. Rev.* B **62** R6093
[24] Gehivelder L, Abrego Castillo I, Gusmao M A, Alonso J A and Cohen L F 1999 *Phys. Rev.* B **60** 12184
[25] Hamilton J J, Keatley E L, Ju H L, Raychaudhuri A K, Smolyaninova V N and Greene R L 1996 *Phys. Rev.* B **54** 14926
[26] Okuda T, Tomioka Y, Asamitsu A and Tokura Y 2000 *Phys. Rev.* B **61** 8009
[27] Schiffer P, Ramirez A P, Bao W and Cheong S-W 1995 *Phys. Rev. Lett.* **75** 3336
[28] Chen X J, Habermeier H U, Zhang C L, Zhang H and Almasan C C 2003 *Phys. Rev.* B. **67** 134405
[29] Kubo K and Ohata N 1972 *J. Phys. Soc. Japan* **33** 21
[30] Li G, Zhou H D, Feng S J, Fan X J and Li X G 2002 *J. Appl. Phys.* **92** 1406